Laser and Particle Beams (2007), *25*, 415–423. Printed in the USA.

DOI: 10.1017/S0263034607000535

Theoretical and experimental studies of the radiative properties of hot dense matter for optimizing soft X-ray sources

N. YU. ORLOV,[1] S. YU. GUS'KOV,[2] S.A. PIKUZ,[2] V.B. ROZANOV,[2] T.A. SHELKOVENKO,[2] N.V. ZMITRENKO,[3] AND D.A. HAMMER[4]

[1]Joint Institute for High Temperatures RAS, Institute for High Energy Density, Moscow, Russia
[2]P.N. Lebedev Physical Institute RAS, Moscow, Russia
[3]Institute of Mathematical Modelling RAS, Moscow, Russia
[4]Laboratory of Plasma Studies, Cornell University, Ithaca, New York

(RECEIVED 15 February 2007; ACCEPTED 21 May 2007)

Abstract

Theoretical and experimental studies of radiative properties of hot dense plasmas that are used as soft X-ray sources have been carried out depending on the plasma composition. Important features of the theoretical model, which can be used for complex materials, are discussed. An optimizing procedure that can determine an effective complex material to produce optically thick plasma by laser interaction with a thick solid target is applied. The efficiency of the resulting material is compared with the efficiency of other composite materials that have previously been evaluated theoretically. It is shown that the optimizing procedure does, in practice, find higher radiation efficiency materials than have been found by previous authors. Similar theoretical research is performed for the optically thin plasma produced from exploding wires. Theoretical estimations of radiative efficiency are compared with experimental data that are obtained from measurements of X-pinch radiation energy yield using two exploding wire materials, NiCr and Alloy 188. It is shown that theoretical calculations agree well with the experimental data.

Keywords: Hot dense plasma; Rosseland and Planck mean free paths

1. INTRODUCTION

The physics of inertial confinement fusion with different ignition scenarios, including fast ignition is a field of very active research, experimentally as well as in theory (Batani *et al.*, 2007; Bret & Deutsch, 2006; Gus'Kov, 2005; Hora, 2007; Ng *et al.*, 2005; Sakagami *et al.*, 2006; Sasaki *et al.*, 2006; Someya *et al.*, 2006). During the heating and compression phase, matter is transformed into a high energy density state. A deeper understanding of the physical processes here, in basic plasma diagnostics and other fields as well, requires reliable data on the radiative opacity of hot dense plasmas (Adamek *et al.*, 2006). Of primary concern are spectrally-dependent coefficients of X-ray absorption, the heat conductivity coefficient, and the Rosseland and Planck mean free paths (Zeldovich & Raizer, 1966). In the field of "indirect-drive" inertial confinement fusion (ICF), soft X-rays (SXR) produced as a result of laser interaction with so-called hohlraum wall are used to implode the capsule containing the fusion fuel. The immediate source of X−rays is the hot dense plasma that is produced by the laser. Some peculiarities of indirectly driven ICF target designs were discussed in previous publications (Denisov *et al.*, 2005; Borisenko *et al.*, 2003; Kilkenny *et al.*, 2005; Koresheva *et al.*, 2005; Kyrala *et al.*, 2005).

X pinch plasma is a SXR source, in which the hot dense plasma is produced as a result of the explosion of fine metal wires (Zakharov *et al.*, 1982; Shelkovenko *et al.*, 2001; Zou *et al.*, 2006). It is produced by using two (or more) wires mounted so that they cross and touch at a single point, in the shape of an "X," as the load of the pulsed power generator. In that case, bright, X-ray emitting micropinches are reliably formed close to the cross point for a wide range of wire materials, wire diameters, and current pulse parameters (Shelkovenko *et al.*, 2001).

In both hohlraum wall plasmas and X pinch plasmas, the radiative characteristics are defined by plasma temperature T,

Address correspondence and reprint requests to: N. Yu. Orlov: Joint Institute for High Temperatures RAS, Institute for High Energy Density, 13/19 Izhorskaya, 127412, Moscow.

plasma density ρ, and plasma composition. For these two plasmas, the latter is determined by the hohlraum wall composition, and the exploding wire composition, respectively. The dependence of the radiative characteristics of the plasma on the X-ray source materials is the subject of the present paper.

The theoretical part of this paper gives a brief overview of different models used to calculate the radiative opacity of hot dense plasmas. Important features of the model used here are described. Two different physical approximations are proposed to estimate radiation efficiency for optically thick and optically thin plasmas, respectively. An optimizing procedure that can determine an effective complex material for producing optically thick plasma by laser interaction with a thick solid target is used. The radiation efficiency of the resulting material is compared with the efficiencies of different materials that have already been estimated theoretically (Suter *et al.*, 1999; Callahan-Miller & Tabak, 2000).

For optically thick plasmas, the Rosseland and Planck mean-free-paths are calculated for two commonly-used exploding wire materials, NiCr and Alloy 188, at fixed temperature and different densities. Theoretical estimates of radiative efficiency are compared with experimental data that were obtained using X pinch plasmas. The experimental part of the present paper describes experimental methods and tools, and presents experimental results on measurements of X-pinch radiation energy yield for the above two wire materials. Theoretical discussion of the results is also presented.

2. THEORETICAL APPROACH

Up to now, several theoretical models and corresponding computer codes have been developed to calculate the spectral coefficients for X-ray absorption, the heat conductivity coefficient, the Rosseland and Planck mean free paths, and other plasma characteristics. Comparative analysis of the Thomas-Fermi model (TF) (Feynman *et al.*, 1949), the Hartree-Fock-Slater model (HFS) (Rozsnyai, 1972; Nikiforov & Uvarov, 1973), the detail configuration accounting (DCA) (Rozsnyai, 1982), and the ion model (IM) (Orlov, 1997) has been carried out based upon the density-functional theory (Orlov & Fortov, 2001), and a brief review of the models is available (Orlov, 2002). The general set of self-consistent field equations that describe the state of the whole ensemble of plasma atoms and ions has been obtained (Orlov & Fortov, 2001). The main feature of this set is the general coupling of all equations for all plasma atoms and ions, including exited states. At first sight, the set cannot be solved because of huge number of equations. Until recently, further physical approximations were used to simplify these equations.

It is necessary to keep in mind that any simplification of the equations leads to a restricted range over which the model can be applied (Orlov & Fortov, 2001). Thus, the TF model can be used only for very high plasma temperatures. The main feature of the HFS model is its average atom approximation, a fictitious atomic system with no integer numbers of bound electrons in the atomic shells. These numbers are calculated using the Fermi-Dirac formula. Because the temperature of the plasma decreases as it radiates, this model cannot provide accurate enough results. The limitation of this approach is connected with the application of perturbation theory, which is used to calculate the properties of a real atomic or ion system. The DCA model uses the Hartree-Fock equations for real atomic and ionic systems, and the Saha method for calculating their concentrations. This approach leads to an arduous problem for high-Z chemical elements (Rozsnyai, 1982). Moreover, it cannot be used for strongly coupled plasmas because of a peculiarity of the Saha method. In reality, the Saha distribution is merely a special case of Gibbs statistics.

Thus, one can indicate the range of plasma temperatures and densities over which the TF, HFS, and DCA models cannot provide accurate enough results because the corresponding additional physical approximations are invalid. Of course, the mentioned ranges are different for different chemical elements (Orlov & Fortov, 2001).

The solution of the general set of self-consistent field equations that describe the state of the whole ensemble of plasma atoms and ions is the way to solve the problem in general. The IM of hot dense plasma (Orlov, 1997) has been developed to achieve this aim. Although more complicated than previous models, the set of equations was solved for "pure" substances. Subsequently, it was applied to compound chemical compositions (Orlov, 1987). As a result, reliable quantum mechanical calculations of radiative opacity became possible over a wide range of plasma densities, and temperatures. Finally, the optimization problem was solved for compound plasma compositions (Orlov, 1999; Denisov et al., 2005). A specific theoretical method and effective computer code were created to optimize radiation spectral yield from complex materials that can be used as X-ray source materials in practice. Theoretical efficiencies of X-ray source materials can be estimated for both optically thick and optically thin plasma.

2.1. Optically thick plasma

Optically thick plasma can be produced by laser interaction with a thick solid target. The simple solution of the steady-state heat conductivity equation in one-dimensional semi-infinite geometry (Orlov, 1999) shows that radiation intensity on the surface of a thick target, $B(T)$ which can be expressed as $B(T) = aT^4$, increases inversely proportional to the Rosseland mean free path, l_R(cm)

$$B(T) \propto \frac{1}{l_R}. \tag{1}$$

Here T is the plasma temperature, $a = 1/15\pi^2 k_B^4/\hbar^3 c^3$, k_B and $\hbar$ are Boltzmann's and Planck's constants, respectively, and c is the speed of light (Denisov *et al.*, 2005). This approximate formula can be used to estimate the radiation

https://doi.org/10.1017/S0263034607000535 Published online by Cambridge University Press

efficiency of a target material. As shown in Eq. (1), the power density increases with decreasing Rosseland mean free path l_R. The relative radiation intensity at a given temperature of two different materials α and β can be expressed as

$$k = \frac{B_\beta(T)}{B_\alpha(T)} = \frac{l_R^\alpha}{l_R^\beta}. \quad (2)$$

A more precise approach was used by Orzechowski *et al.* (1996) for evaluating the radiation energy lost into the thick target. A self-similar solution for the diffusion equation gives the energy lost to the wall ΔE increases inversely proportional to the square root of the Rosseland mean opacity k_R, where $k_R = 1/\mathrm{l}_R\tilde{\rho}$, and $\tilde{\rho}(g/cm^3)$ is the plasma density:

$$\Delta E = \left[\frac{1}{K_R}\right]^{1/2} = [l_R\tilde{\rho}]^{1/2}. \quad (3)$$

The radiation efficiency of a target material surface increases with a reduction of the energy transported into the wall ΔE. It can be achieved by increasing the Rosseland mean opacity k_R, or, at fixed plasma density, by decreasing the Rosseland mean free path l_R. In this case, estimating the relative energy lost to the wall of two different materials α and β can be expressed as

$$\frac{\Delta E_\beta}{\Delta E_\alpha} = \left[\frac{l_R^\beta}{l_R^\alpha}\right]^{1/2} \quad (4)$$

The value ΔE in Eq. (3) should be minimized to achieve the maximum surface radiation efficiency. Eq. (4) will be used below to estimate relative efficiency of different wall materials. Radiation efficiency clearly increases with decreasing Rosseland mean free path.

2.2. Optically thin plasma

Another approach can be used for estimating the emissive of optically thin plasma that can be produced by exploding wires. Let a one-dimensional (1D) planar plasma slab have the thickness L and occupy $0 \le x \le L$. It has been proved (Zeldovich & Raizer, 1966), in the absence of external sources, that the integrated surface emissive, or outward energy flux, on the right border of the slab, where $x = L$, increases inversely proportional to the Planck mean free path l_P

$$j^+ \propto \frac{L}{l_P} caT^4. \quad (5)$$

The applicability range of the approximation may be expressed as $\tilde{L} < l_P$.

Eq. (5) can be used to estimate relative radiation efficiency of different exploding wires made of two different materials α and β:

$$k = \frac{j_\alpha^+}{j_\beta^+} = \frac{l_P^\beta}{l_P^\alpha}. \quad (6)$$

This approximate equation will be used below to compare theoretical and experimental results.

Thus, radiation efficiency increases with decreasing Rosseland or Planck mean free path for optically thick or optically thin plasma, respectively. Therefore, an optimal chemical composition for optically thick plasmas can be achieved by minimizing the Rosseland mean free path. In case optically thin plasmas, the Planck mean free path should be minimized.

2.3. Results of calculations

Chemical admixtures can considerably influence the frequency-dependent opacity, as has been previously shown. This fact can be used to improve the radiation efficiency of X-ray source materials. For instance, a simple 50/50 mixture of gold and gadolinium was proposed to reduce the radiation energy lost to the hohlraum walls in comparison with pure gold (Orzechowski *et al.*, 1996).

Table 1 presents the Rosseland mean free paths l_R, which were calculated for different materials at the density $\tilde{\rho} = 1/g/cm^3$) and different temperatures, using the IM of hot dense plasma. Results are given for gold and for the composition (Au25.7%/W23.1%/Gd18.1%/Pr10.0%/Ba10.4%/Sb12.7%), which is denoted as Composition 1. Mass percentages of elements are given in brackets. This composition was found using an optimization method (Denisov *et al.*, 2005) that is more complete than that of Orlov (1999). Results are also presented for two compositions of gold and gadolinium. The problem is that the notation 50/50, which was used

Table 1. *The Rosseland mean free path (cm) calculated for different materials at the density* $\tilde{\rho} = 1(g/cm^3)$

T(eV)	Au	Comp. 1.	l_R^{Au}/l_R^{Comp1}	Au55.61/Gd44.39 (Comp. 2)	l_R^{Au}/l_R^{Comp2}	Au50/Gd50 (Comp. 3)	l_R^{Au}/l_R^{Comp3}
150	3.2110^{-4}	1.2910^{-4}	2.49	2.4610^{-4}	1.30	2.4710^{-4}	1.29
200	4.5710^{-4}	1.5310^{-4}	2.98	3.2910^{-4}	1.39	3.2910^{-4}	1.39
250	5.0110^{-4}	1.6110^{-4}	3.11	2.8810^{-4}	1.74	2.8910^{-4}	1.73
300	5.7510^{-4}	1.8710^{-4}	3.07	3.7610^{-4}	1.53	3.8910^{-4}	1.48
350	6.3510^{-4}	1.9210^{-4}	3.31	4.2510^{-4}	1.49	4.3710^{-4}	1.45

https://doi.org/10.1017/S0263034607000535 Published online by Cambridge University Press

earlier (Orzechowski et al., 1996), could mean number or mass percentages. Therefore, calculations were made here both for Composition 2 (Au55.61%/Gd44.39%) and for Composition 3 (Au50%/Gd50%) where, again, we have used mass fraction.

The spectral coefficients for X-ray absorption, $K(x)(\mathrm{cm}^2/\mathrm{g})$, were calculated for different compositions at $T = 250$ eV and $\tilde{\rho} = 1 g/cm^3$ as functions of $x = \hbar\omega/T$. Figure 1 presents the coefficient calculated for gold (thick line). The coefficient is relatively small in the interval $(3.5 < x < 8.5)$ whereas the interval is overlapped with spectral lines for Composition 1 (thin line). Figure 2 shows the spectral coefficients for X-ray absorption calculated for gold and Composition 2 (Au55.61%/Gd44.39%). One can see that Composition 2 also ensures definite overlapping over the previously-cited energy interval. However, Composition 1 provides broader overlapping than Composition 2, as shown in Figure 3.

Table 2 presents the relative hohlraum wall loss energy for different materials compared to a pure gold hohlraum wall as calculated by Suter *et al.* (1999), as well as some results from the present work, including Composition 1. Table 3 presents the relative hohlraum wall loss energy for different materials as compared to a gold/ gadolinium hohlraum wall as calculated by Callahan-Miller and Tabak (2000). The result of the present work is also given (Composition 1). Tables 2 and 3 show that Composition 1 ensures higher radiation efficiency in comparison with other calculated compositions. Thus, the optimizing procedure (Denisov *et al.*, 2005), which can find out an effective complex material for a thick target, really can lead to better radiation efficiency materials.

The Rosseland and Planck mean free paths were also calculated for the NiCr alloy (Ni80%/Cr20%) and for Alloy 188 (Cr21.72%/Ni22.92%/Fe2.24%/Co39%/W13.93%) at the temperature $T = 1$ keV. Calculations were made at normal density $\tilde{\rho} = \tilde{\rho}_{normal}$ (g/cm^3), at the density $\tilde{\rho} = 0.1*\tilde{\rho}_{normal}$ (g/cm^3) and at the density $\tilde{\rho} = 10*\tilde{\rho}_{normal}$ (g/cm^3) (Tables 4 and 5).

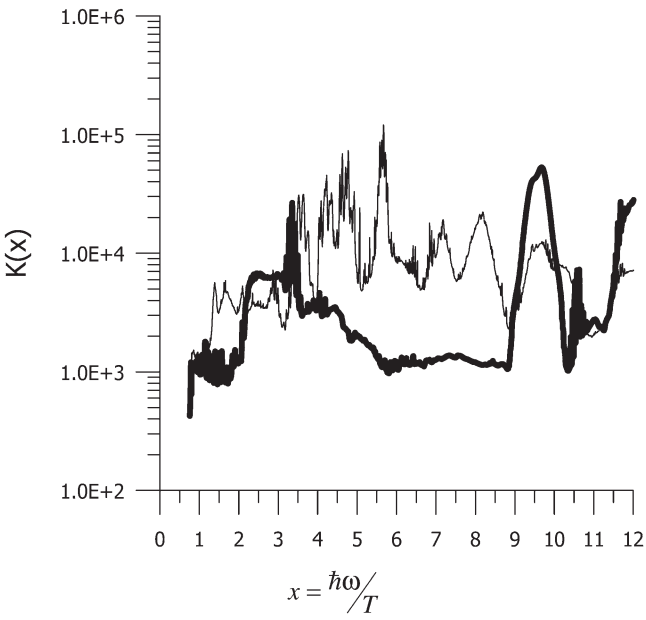

Fig. 1. The spectral coefficient of X-rays absorption $K(x)(cm^2/g)$ calculated for Au (thick line) and for the Composition 1 (Au25.7%/W23.1%/Gd18.1%/Pr10.0%/Ba10.4%/Sb12.7%) (thin line) at the temperature T = 250 eV and the density $\tilde{\rho} = 1\ \mathrm{g}/cm^3$.

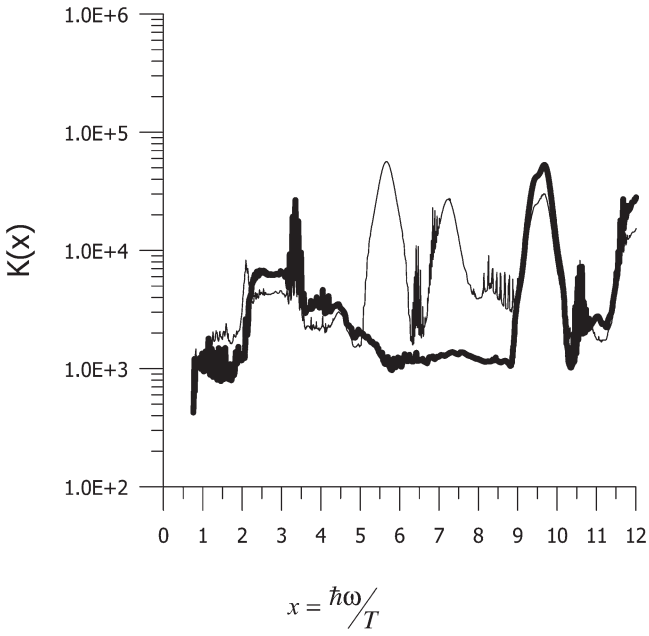

Fig. 2. The spectral coefficient of X-rays absorption $K(x)(cm^2/g)$ calculated for Au (thick line) and for the Composition 2 (Au55.61%/Gd44.39%) (thin line) at the temperature T = 250 eV and the density $\tilde{\rho} = 1\mathrm{g}/cm^3$

Figure 4 presents the spectral coefficients for X-ray absorption $K(x)(cm^2/g)$ calculated for the NiCr alloy and Alloy 188 at the temperature $T = 1$ keV and the density $\tilde{\rho} = \tilde{\rho}_{normal}$ (g/cm^3). The spectral coefficients for X-ray absorption of NiCr (thick line) are relatively small over the interval $(2.0 < x < 5.5)$. On the other hand, the interval is overlapped with spectral lines of Alloy 188 (thin line). These circumstances provide decreasing Rosseland and Planck mean free paths for Alloy 188 in comparison with

Table 2. *The hohlraum wall loss energy for different materials, compared to a Au hohlraum wall* $\Delta E_{wall}/\Delta E_{Au}$

Material	$\Delta E/\Delta E_{\mathrm{Au}}$
Au	1.00
Au:Gd	0.83
U:At:W:Gd:La	0.65
U:Bi:W:Gd:La	0.65
U:Bi:Ta:Dy: Nd	0.63
Th:Bi:Ta:Sm:Cs	0.68
U:Pb:Ta:Dy:Nd	0.63
U:Ta:Dy:Nd:	0.67
U:Au:Ta:Dy:Nd	0.64
U:Nb.14:Au:Ta:Dy	0.66
Composition 1	0.57

https://doi.org/10.1017/S0263034607000535 Published online by Cambridge University Press

Table 3. *The hohlraum wall loss energy for different materials, compared to a AuGd hohlraum wall* $\Delta E_{wall}/\Delta E_{AuGd}$

Material	$\Delta E_{wall}/\Delta E_{AuGd}$
Au/Gd (50:50)	1.00
Au	1.25
Pb	1.28
Hg	1.26
Ta	1.25
W	1.25
Pb/Ta (50:50)	1.08
Pb/Ta (70:30)	1.06
Hg/Xe (50:50)	1.18
Pb/Ta/Cs (50:20:30)	1.01
Pb/Ta/Cs (45:20:35)	1.01
Hg/Ta/Cs (45:20:35)	1.03
Hg/W/Cs (45:20:35)	1.04
Pb/Hf (70:30)	1.04
Pb/Hf/Xe (45:20:35)	1.00
Composition 1	0.75

NiCr and, therefore, improve the radiation efficiency of the corresponding wire material.

The results in Tables 4 and 5 will be compared with experimental measurements in the next section after a description of the experiments.

3. EXPERIMENTAL RESULTS

To compare the calculations, above, to the real hot plasmas requires knowledge of the plasma temperature, density,

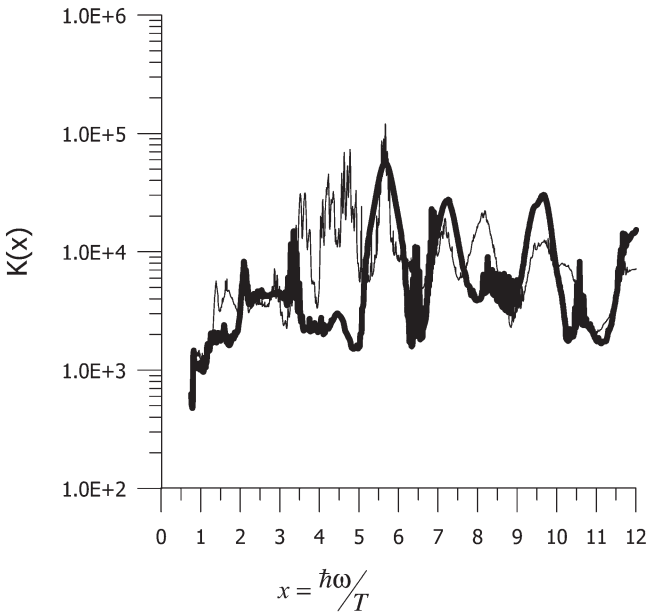

Fig. 3. The spectral coefficient of X-rays absorption $K(x)(cm^2/g)$ calculated for the Composition 2 (Au55.61%/Gd44.39%) (thick line) and for the Composition 1 (Au25.7%/W23.1%/Gd18.1%/Pr10.0%/Ba10.4%/Sb12.7%) (thin line) at the temperature T = 250 eV and the density $\rho = 1 g/cm^3$.

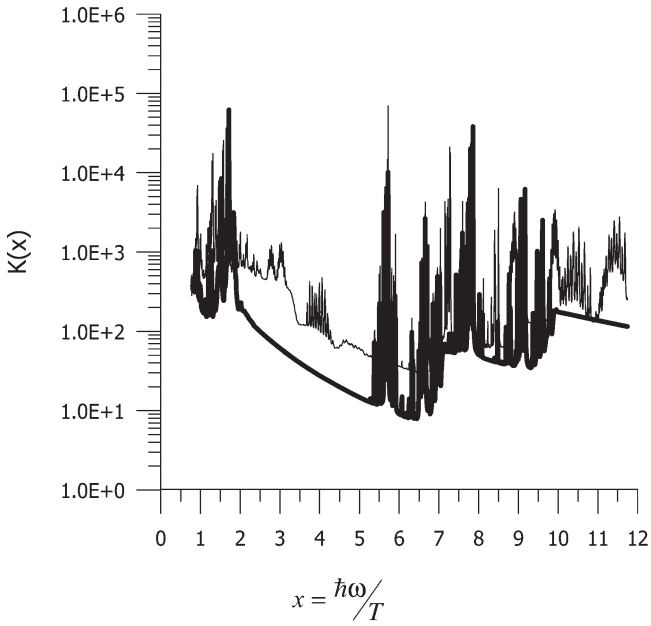

Fig. 4. The spectral coefficient of X-rays absorption $K(x)(cm^2/g)$ calculated for NiCr (thick line) and for the composition Alloy 188 (Cr21.72%/Ni22.92%/Fe2.24%/Co39%/W13.93%) (thin line) at the temperature T = 1 keV and the density $\tilde{\rho} = \tilde{\rho}_{normal}$.

radiated energy, size, etc. In an exploding wire *z* pinch, a high current is passed through a single fine wire (10–100 μm in diameter and ~1 cm long) that connects the output electrodes of a pulsed power generator. The wire explodes and is converted into plasma by the rising current pulse, after which the increasing self-magnetic field can cause the plasma to implode radically. This process typically yields several bright, X-ray emitting micro-pinches at random locations along the wire, which limits the opportunities to make precise measurements of plasma parameters of an

Table 4. *The Rosseland mean free path (cm) calculated for NiCr and Alloy 188 at the temperature T = 1 keV*

Density	l_R^{NiCr}	$l_R^{Alloy188}$	$k = l_R^{NiCr}/l_R^{Alloy188}$
$0.1*\tilde{\rho}_{normal}$	2.5410^{-1}	1.9710^{-2}	12.89
$\tilde{\rho}_{normal}$	4.1210^{-3}	1.3710^{-3}	3.01
$10.*\tilde{\rho}_{normal}$	1.1110^{-4}	5.8110^{-5}	1.91

Table 5. *The Planck mean free path (cm) calculated for NiCr and Alloy 188 at the temperature T = 1 keV*

Density	l_P^{NiCr}	$l_P^{Alloy188}$	$k = l_P^{NiCr}/l_P^{Alloy188}$
$0.1*\tilde{\rho}_{normal}$	1.1610^{-2}	2.8310^{-3}	4.06
$\tilde{\rho}_{normal}$	2.9910^{-4}	2.1610^{-4}	1.38
$10.*\tilde{\rho}_{normal}$	3.2910^{-5}	1.7810^{-5}	1.84

https://doi.org/10.1017/S0263034607000535 Published online by Cambridge University Press

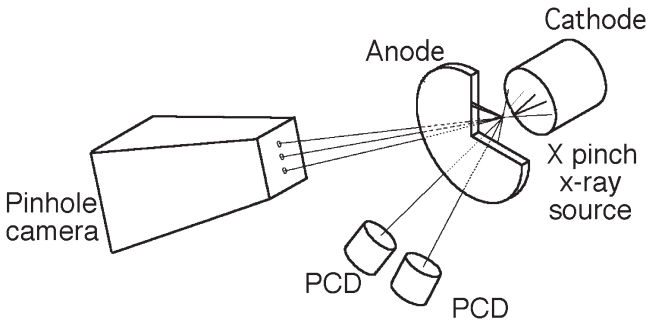

Fig. 5. Experimental setup for measurement of the X pinch source radiated energy.

individual X-ray source (Zakharov *et al.*, 1983). An X pinch, produced as described in the Introduction (Zakharov *et al.*, 1982; Shelkovenko *et al.*, 2001), by contrast, reliably produces X-ray emitting micro-pinches close to the cross point of the two wires for a wide range of wire materials, wire diameters, and current pulse parameters (Shelkovenko *et al.*, 2001). Therefore, the X pinch enables the physical properties of micro-pinches to be investigated in detail by predetermining their location to within about 150 μm. Thus, diagnostic instruments can be focused on the wire cross point region and many kinds of diagnostics can be used. The X pinches radiate over a wide range of X-ray energies, and the size of the radiation region varies from 1 mm to 1 μm in diameter, depended on the wire material and energy. The wide spectral range of the radiated energy from a small area and a predictable location offer the possibility of using the X pinch as source of X-ray radiation for different applications, including detailed studies of X-ray spectral emission characteristics.

The experimental results reported here were obtained using the XP facility (470 kA peak current, 100 ns full-width at half-maximum (FWHM) pulse duration) at Cornell University. A simplified schematic diagram of the experimental configuration and diagnostics is shown in Figure 5 for the case of a single four-wire X pinch. The set of diagnostics used in the experiments with X pinches in recent years (Shelkovenko *et al.*, 2001; Song *et al.* 2005), shows that a $\sim$1–10 μm plasma source with $\geq$1 keV plasma temperature, and density equal to 0.1–1 of solid density radiates in the $>$1 keV energy range. These plasma parameters were used for radiative opacity calculation.

The pulse duration, shape, and radiated energy of the X-ray bursts were measured in the 1.0–6 keV band using fast diamond photo conducting detectors (PCDs), as shown in Figure 5. For most of the experiments the X-ray radiation bursts from the X pinches were monitored using two or three PCDs and a 5 GS/s Tektronix 684B digitizing oscilloscope. Including the cabling, this combination gave $\geq$0.5 ns X-ray pulse widths (FWHM) and timing accuracy of $\pm$0.2 ns for most tests. The PCDs were calibrated so that radiated power and energy estimates could be made from them. Different filter combinations were used to obtain power and energy estimates with different minimum photon energies.

Table 6. *Energy radiated of 4 × 25 μm NiCr and 4 × 25 μm alloy 188 X pinches in the two energy bends*

4 × 25 μm NiCr X pinch		4 × 25 μm Alloy 188 X pinch	
Pulse #	B_1^{NiCr} (mJ) E$\gamma >$ 1.5 keV	Pulse #	$B_1^{Alloy188}$ (mJ) E$\gamma >$ 1.5 keV
3620	320	3673	480
3626	360	3676	600
3629	300	3679	620
$\bar{B}_1^{NiCr}$	326	$\bar{B}_1^{Alloy188}$	566
Pulse #	B_2^{NiCr} (mJ) 2.5 $<$ E$\gamma <$ 5 keV	Pulse #	$B_2^{Alloy188}$ (mJ) 2.5 $<$ E$\gamma <$ 5 keV
3620	140	3673	250
3626	100	3676	210
3629	90	3679	170
$\bar{B}_2^{NiCr}$	110	$\bar{B}_2^{Alloy188}$	210

Table 7. *Theoretical and experimental results on relative radiation efficiency of exploding wires made of Alloy 188 and NiCr. Experimental results are given as* $\bar{B}_1^{Alloy188}/\bar{B}_1^{NiCr}$

Experiment (E $>$ 1.5 keV)		Theory		
$\bar{B}_1^{Alloy188}/\bar{B}_1^{NiCr}$	Error bar	$k = l_P^{NiCr}/l_P^{Alloy188}$		Deviation from experiment
1.736	20%	$\tilde{\rho} = \tilde{\rho}_{normal}$	1.38	25.8%
		$\tilde{\rho} = 10.*\tilde{\rho}_{normal}$	1.84	5.6%

https://doi.org/10.1017/S0263034607000535 Published online by Cambridge University Press

Table 8. *Theoretical and experimental results on relative radiation efficiency of exploding wires made of Alloy 188 and NiCr. Experimental results are given as* $\bar{B}_2^{Alloy188}/\bar{B}_2^{NiCr}$.

Experiment ($2.5 < E < 5$ keV)		Theory		
$\bar{B}_2^{Alloy188}/\bar{B}_2^{NiCr}$	Error bar	$k = l_P^{NiCr}/l_P^{Alloy188}$		Deviation from experiment
1.9	20%	$\tilde{\rho} = \tilde{\rho}_{normal}$	1.38	37.7%
		$\tilde{\rho} = 10.*\tilde{\rho}_{normal}$	1.84	3.2%

The PCDs were placed as far as 43 cm from the X pinch. Because of the small size of the X pinch radiating source (Shelkovenko *et al.*, 2001; Song *et al.*, 2007), we can consider that the X pinch is a point source of radiation radiating uniformly in all direction.

We reported here only the results from four wires X pinches from NiCr and Alloy 188. Radiated energy estimated using PCDs signals with Be and Ti filters for NiCr and Alloy 188 four-wire X pinches was averaged for several pulses in Table 6. We used for calculation only pulses with similar current and dI/dt to get comparable energy yield. According to Table 6, the averaged radiated energy ratios of NiCr and alloy 188 X pinches are 1.75 and 1.88 for $E\gamma > 1.5$ keV and $2.5 < E\gamma < 5$ keV, respectively.

Our spectroscopic and imaging experiments have shown micrometer scale source size and plasma density near solid density in the energy range more than 1.5 keV. Magnetic hydro dynamics simulations show even 10 times higher density than has been measured by spectroscopy methods (Gus'kov *et al.*, 2005). Therefore, we compare the experimental results assuming solid density and 10 times of solid density with calculations presented in Tables 4 and 5. Because of small size, the X pinch source of radiation is an optically thin source over the energy range of interest. The ratio of the energy radiated by Alloy 188 to the energy radiated by the NiCr alloy in the energy ranges studied fits the relation of the Planck mean free paths to these alloys quite well for densities between $\tilde{\rho}_{normal}$ and $10.*\tilde{\rho}_{normal}$.

Tables 7 and 8 compares theoretical (Table 5) and experimental (Table 6) results concerning relative efficiency of exploding wires made of Alloy 188 and NiCr. As shown, theoretical results agree well with the experimental data.

4. CONCLUSIONS

It is shown that the theoretical method presented in this paper, provides reasonable results on estimating the radiation efficiency of X-ray source materials. This method can be used to determine effective complex materials for exploding wires, thick laser targets, and other applications. The method can also reduce expenses and time of pure experimental research. This is especially important for experiments on the biggest installations such as the Sandia ZR pulsed power machine or the National Ignition Facility laser.

ACKNOWLEDGEMENTS

This work was performed with support of RFBR 05-02-17532) and Department of Energy under Grant No. DE-FG03-98ER54496.

REFERENCES

Adamek, P., Renner, O., Drska, L., Rosmej, F.B. & Wyart, J.F. (2006). Genetic algorithms in spectroscopic diagnostics of hot dense plasmas. *Laser Part. Beams* **24**, 511–518.

Batani, D., Dezulian, R., Redaelli, R., Benocci, R., Stabile, H., Canova, F., Desai, T., Lucchini, G., Krousky, E., Masek, K., Pfeifer, M., Skala, J., Dudzak, R., Rus, B., Ullschmied, J., Malka, V., Faure, J., Koenig, M., Limpouch, J., Nazarov, W., Pepler, D., Nagai, K., Norimatsu, T. & Nishimura, H. (2007). Recent experiments on the hydrodynamics of laser-produced plasmas conducted at the PALS laboratory. *Laser Part. Beams* **25**, 127–141.

Borisenko, N.G., Akunets, A.A., Bushuev, V.S., Dorogotovtsev, V.M. & Merkuliev, Y.A. (2003). Motivation and fabrication methods for inertial confinement fusion and inertial fusion energy targets. *Laser Part. Beams* **21**, 505–509.

Bret, A. & Deutsch, C. (2006). Density gradient effects on beam plasma linear instabilities for fast ignition scenario. *Laser Part. Beams* **24**, 269–273.

Callahan-Miller, D. & Tabak, M. (2000). Progress in target physics and design for heavy ion fusion. *Phys. Plasmas* **7**, 2083–2091.

Denisov, O.B., Orlov, N. Yu., Gus'kov, S. Yu., Rozanov, V.B., Zmitrenkop, N.V. & Michailov, A.P. (2005). Modelling of the composition of materials for soft X-ray sources used in research on inertial confinement fusion. *Plasma Phys. Rep.* **31**, 684–689.

Feynman, R., Metropolis, N. & Teller, E. (1949). Equations of state of elements based on the generalized Fermi-Thomas theory. *Phys. Rev.* **75**, 73–79.

Gus'kov, S.Yu., Ivanenkov, G.V. & Stepnievski, W. (2005). Physical aspects of high intensity emission from X-pinch. *Proc. SPIE* **5974**, 59740T1–10.

Gus'Kov, SY. (2005). Thermonuclear gain and parameters of fast ignition ICF-targets. *Laser Part. Beams* **23**, 255–260.

Hora, H. (2007). New aspects for fusion energy using inertial confinement. *Laser Part. Beams* **25**, 37–45.

Kilkenny, J.D., Alexander, N.B., Nikroo, A., Steinman, D.A., Nobile, A., Bernat, T., Cook, R., Letts, S., Takagi, M. & Harding, D. (2005). Laser targets compensate for limitations in inertial confinement fusion drivers. *Laser Part. Beams* **23**, 475–482.

https://doi.org/10.1017/S0263034607000535 Published online by Cambridge University Press

Koresheva, E.R., Osipov, I.E. & Aleksandrova, I.V. (2005). Free standing target technologies for inertial fusion energy: Target fabrication, characterization, and delivery. *Laser Part. Beams* **23**, 563–571.

Kyrala, G.A., Delamater, N., Wilson, D., Guzik, J., Haynes, D., Gunderson, M., Klare, K., Watt, R.W., Wood, W.M. & Varnum, W. (2005). Direct drive double shell target implosion hydrodynamics on OMEGA. *Laser Part. Beams* **23**, 187–192.

Ng, A., Ao, T., Perrot, F., Dharma-Wardana, M.W.C. & Foord, M.E. (2005). Idealized slab plasma approach for the study of warm dense matter. *Laser Part. Beams* **23**, 527–537.

Nikiforov, A. & Uvarov, V. (1973). Opisanie sostoyaniya veschestva v oblasti visokoch temperatur na osnove uravnenii samosoglasovannogo polya. *Chislennye metodi mech. sploscnoi sredi*. **4**, 114–117 (in Rusian).

Orlov, N. Yu. & Fortov, V.E. (2001). Comparative analysis of the theoretical models of a hot dense plasma and the density functional theory. *Plasma Phys. Rep.* **27**, 44–55.

Orlov, N. Yu. (1987). Quantum statistical calculations of the properties of a mixture of chemical elements allowing for fluctuations in the occupation numbers of electron states. *USSR Comput. Math. Phys.* **27**, 64–70.

Orlov, N. Yu. (1997). Ion model of a hot dense plasma. *Laser Part. Beams* **15**, 627–634.

Orlov, N. Yu. (1999). Calculation of the radiative opacity of a hot dense plasma. *Contrib. Plasma Phys.* **39**, 177–180.

Orlov, N. Yu. (2002).Theoretical models of hot dense plasmas for inertial confinement fusion. *Laser Part. Beams* **20**, 547–549.

Orzechowski, T.J., Rosen, M.D., Korblum, M.D., Porter, J.L., Suter, L.J., Thissen, A.R. & Wallace, R.J. (1996). The Rosseland mean opacity of a mixture of gold and gadolinium at high temperatures. *Phys. Rev. Lett*. **77**, 3545–3548.

Rozsnyai, B.F. (1972). Relativistic Hartree-Fock-Slater calculations for arbitrary temperature and matter density. *Phys. Rev*. **5**, 1137–1149.

Rozsnyai, B.F. (1982). An overview of the problems connected with theoretical calculations for hot plasmas. *J. Quant. Spectrosc. Radiat. Trans.* **27**, 3, 211–217.

Sakagami, H., Johzaki, T., Nagatomo, H. & Mima, K. (2006). Fast ignition integrated interconnecting code project for cone-guided targets. *Laser Part. Beams* **24**, 191–198.

Sasaki, T., Yano, Y., Nakajima, M., Kawamura, T. & Horioka, K. (2006). Warm-dense-matter studies using pulse-powered wire discharges in water. *Laser Part. Beams* **24**, 371–380.

Shelkovenko, T.A., Sinars, D.B., Pikuz, S.A. & Hammer, D.A. (2001). Radiographic and spectroscopic studies of X pinch plasma implosion dynamics and X-ray burst emission characteristics. *Phys. Plasma* **8**, 1305–1318.

Someya, T., Miyazawa, K., Kikuchi, T. & Kawata, S. (2006). Direct-indirect mixture implosion in heavy ion fusion. *Laser Part. Beams* **24**, 359–369.

Song, B.M., Pikuz, S.A. & T.A. Shelkovenko, T.A. (2005). Determination of the size and structure of an X pinch X-ray source from the diffraction pattern produced by microfabricaterd slits. *Appl. Opt*. **44**, 2349–2358.

Suter, L., Rothenberg, J., Munro, D., Van Wonterghem, B., Haan, S., & Lindl, J. (1999). Feasibility of High Yield/High Gain NIF capsules. *Proceedings of International Fusion Sciences and Applications*. Paris: Elsevier.

Zakharov, S.M., Ivanenkov, G.V., Kolomenskii, S.A., Pikuz, S.A. & Samokhin, A.I. (1983). Exploding-wire plasma in the diode of a high-current accelerator. *Sov. J. Plasma Phys.* **9**, 271–275.

Zakharov, S.M., Ivanenkov, G.V., Kolomenskii, S.A., Pikuz, S.A., Samokhin, A.I. & Ulshmid, I. (1982). Wire X- pinch in a high-current diode. *Tech. Phys. Lett.* **8**, 456–457.

Zeldovich, J.B. & Raizer, Y.P. (1966). *Phizika udarnich voln i visokotemperaturnich gidrodinamicheskich yavlenii.* M., Nauka. (in Rusian).

Zou, X.B., Liu, R., Zeng, N.G., Han, M., Yuan, J.Q., Wang, X.X. & Zhang, G.X. (2006). A pulsed power generator for x-pinch experiments. *Laser Part. Beams* **24**, 503–509.

APPENDIX

A plasma with a nuclear charge Z, atomic weight A, temperature T, and density $\tilde{\rho}\,(\mathrm{g/cm^3})$ can be considered to define the Rosseland and Planck mean-free-paths l_R and l_P, respectively. An ion sphere of radius r_0 with a nucleus at its center is used as a subsystem of Gibbs statistics (Orlov, 1997). The ion sphere radius is

$$r_0 = \left[\frac{3}{4\pi N_A}\right]^{1/3} \frac{1}{a_0} \left[\frac{A}{\tilde{\rho}}\right]^{1/3}, \tag{7}$$

where $a_0 = 5.29210^{-9}\,\mathrm{cm}$ and $N_A = 6.0210^{23}$, the Avogadro number. An atomic units system is used where the electron charge $e = 1$, Planck's constant $\hbar = 1$, and electron mass $m = 1$. The atomic units of length, time, and energy, respectively, are $\hbar 2/me^2$, $\hbar^3/me^4$, and $me^4/\hbar^2$.

The subsystems differ from each other by sets of numbers of bound electrons $\{N_a^j\}$ on the atomic shells, where j numbers the subsystems, and α denotes the orbital (nl). The Gibbs distribution is

$$W_j = Cg_j \exp\left\{-\frac{E_j - \mu N_j}{T}\right\}. \tag{8}$$

Here, E_j is the total energy and N_j is the total number of electrons in a subsystem with index j: g_j is the statistical weight; μ is the chemical potential.

The Rosseland mean free path l_R can be expressed as

$$l_R = \frac{15}{4\pi^4} \int_0^\infty l_u \frac{u^4 \exp(-u)}{(1-\exp(-u))^2}\, du, \tag{9}$$

where $u = \hbar\omega/T$, $\hbar\omega$ photon energy, $l_u = 1/K(\omega)$. The spectrally-dependent coefficients of X-ray absorption has the form

$$K(\omega) = \tilde{n} \sum_j W_j \sigma^j(\omega), \tag{10}$$

https://doi.org/10.1017/S0263034607000535 Published online by Cambridge University Press

$\tilde{n}$ is the nuclei concentration $(1/cm^3)$. The total cross-section of photon absorption is determined as $\sigma^j(\omega) = \sigma^j_{bb}(\omega) + \sigma^j_{bf}(\omega) + \sigma^j_{ff}(\omega)$, and represents the sum of the cross sections for spectral line absorption $\sigma^j_{bb}(\omega)$, photo absorption $\sigma^j_{bf}(\omega)$ and bremsstrahlung absorption $\sigma^j_{ff}(\omega)$. The processes of scattering and stimulated emission can also be incorporated into formula (10). The Planck mean free path l_P is

$$\frac{1}{l_P} = \frac{15}{\pi^4}\int_0^\infty \frac{1}{l_u}\frac{u^3\exp(-u)}{1-\exp(-u)}du. \tag{11}$$

https://doi.org/10.1017/S0263034607000535 Published online by Cambridge University Press